Multi-Scale Region of Interest Pooling for Facial Action Unit Detection

BY

GUGLIELMO MENCHETTI
B.S, Università degli studi di Firenze, Firenze, Italy, 2017

THESIS

Submitted as partial fulfillment of the requirements
for the degree of Master of Science in Computer Science
in the Graduate College of the
University of Illinois at Chicago, 2020

Chicago, Illinois

Defense Committee:

Ahmet Enis Cetin, Chair and Advisor
Ugo Buy
Elena Zheleva
Mark Carman, Politecnico di Milano

ACKNOWLEDGMENTS

I would like to express my gratitude to my Supervisors, Professor Enis Cetin and Professor Mark Carman, for their constant guidance and support, without which this work would have not been possible. It has been a beautiful journey and an amazing opportunity to take part in the Double Degree program between the University of Illinois at Chicago and Politecnico di Milano.

Also, I would like to thank my parents and friends who have supported me throughout my Master's and have always believed in me. I would like to express the deepest appreciation to Phakphoum, a friend, a mentor an amazing individual who has helped me through my research and personal challenges.

GM

TABLE OF CONTENTS

TABLE OF CONTENTS (continued)

CHAPTER **PAGE**

LIST OF TABLES

LIST OF FIGURES

LIST OF ABBREVIATIONS

AU	Action Unit
FACS	Facial Action Unit Coding System
DL	Deep Learning
SOTA	State-Of-The-Art
CNN	Convolutional Neural Network
CV	Computer Vision
MLP	Multi-Layer Perceptron
FPN	Feature Pyramid Network
RoI	Region of Interest
ML	Machine Learning
SGD	Stochastic Gradient Descent
LR	Learning Rate
DRML	Deep-Region and Multi-Label Learning
EAC	Enhancing And Cropping
FC	Fully Connected
ARL	Attention and Relation Learning
BB	Bounding Box

SUMMARY

Facial expression is the natural mean used by humans to express their intentions and emotions. The main challenge in detecting facial expressions is given by the ambiguities between them.

The Facial Action Unit Coding System (FACS) helps to address the problem of ambiguities between expressions. The FACS consists of deconstructing each expression in a collection of facial muscle movements, also known as Facial Action Units (AU).

In this document, we focus on single-frame Action Unit recognition, in which we aim at detecting the AUs in an image containing a face.

In this work, we will examine the current state-of-the-art (SOTA) on Facial AU detection and we will introduce a novel Deep Learning architecture, that achieves competitive results compared to the current state-of-the-art on a popular benchmark.

Particularly, we will study the impact of Multi-Scale feature construction using Feature Pyramid Network, and the extraction of features related to specific regions of the face through the use of Region Of Interest (RoI) Pooling.

We will compare the obtained results with other state-of-the-art methods and we investigate the effect of the different components of the model enclosing various ablation studies.

In conclusion, we will suggest possible future improvements to the current architecture.

CHAPTER 1

INTRODUCTION

Facial expression is the natural mean used by humans to express their intentions and emotions. The analysis of facial expressions captures the attention of researchers, due to its wide range of potential applications such as medical (pain detection [1; 2], mental health diagnosis [3]), in education [4] and entertainment [5].

However, detecting facial expressions may be challenging due to the ambiguities of expressions. This ambiguity can be solved thanks to the representation of expressions towards the use of the Facial Action Unit Coding System (FACS) [6].

The FACS defines a taxonomy for 46 human facial movements by their change in appearance on the face. The system was first published in 1978 then updated in 2002 and since then has been used by human coders to characterize all the possible facial expressions, by deconstructing them into Facial Action Units (AUs) which are fine-grained facial movements defined for some local regions of the face. The process of AU annotation, however, requires a deep knowledge of the FACS system and a long time to manually annotate entire videos.

In recent years, many FACS coded databases [7; 8; 9; 10] have been released by universities and laboratories, allowing researchers to develop new techniques for automatically annotating facial AUs. Moreover, the advances in Computer Vision related tasks brought by Deep Neural Networks, have made researchers apply neural network techniques to solve the task of AUs detection.

Upper Face Action Units					
 Inner Brow Raiser	 Outer Brow Raiser	 Brow Lowerer	 Upper Lid Raiser	 Cheek Raiser	 Lid Tightener
 Lid Droop	 Slit	 Eyes Closed	 Squint	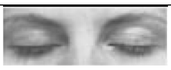 Blink	 Wink

Upper Face Action Units					
 Nose Wrinkler	 Upper Lip Raiser	 Nasolabial Deepener	 Lip Corner Puller	 Cheek Puffer	 Dimpler
 Lip Corner Depressor	 Lower Lip Depressor	 Chin Raiser	 Lip Puckerer	 Lip Stretcher	 Lip Funneler
 Lip Tightener	 Lip Pressor	 Lips Part	 Jaw Drop	 Mouth Stretch	 Lip Suck

TABLE I: Examples of Action Units in the FACS system

Nevertheless, the task of AU detection is not considered solved, since in a real-word environment AU recognition systems are sensible to illumination variation, head pose, and subject-dependence. Furthermore, the similarities between Facial Action Units make this task even more difficult and prone to errors in their recognition.

1.1 Motivations

The scope of this work is to study the problem of Facial AU detection, evaluating both classical methods and the current state-of-the-art. After evaluating the strength and weaknesses of the previous methods, we develop a novel Deep Learning (DL) architecture to solve the AU recognition problem.

In particular, we enhance two well-known techniques used in various AU recognition models. The first one is multi-scale feature extraction, which we implement through the use of a Feature Pyramid Network. The other is the region learning technique, which is accomplished with the introduction of the Region of Interest Pooling module. We show that the implementation of these techniques, allows our model to achieve performances comparable with the current SOTA methods.

1.2 Document Structure

In Chapter 2 we will give some background on the Deep Learning techniques that are used as the base for our model. In Chapter 3 we will give a brief description of the state-of-the-art approaches for AU detection. Chapter 4 describes the structure of our model, providing insight into every single component. In Chapter 5 we detail the training and validation procedures, we describe the available data and the pre-processing techniques that we applied. Finally, in Chapter 6 we report the achieved results, along with ablation studies on different components of the model.

CHAPTER 2

BACKGROUND

2.1 Convolutional Neural Networks

Convolutional Neural Networks (CNN)[11] are a class of deep neural networks, that allowed advancements of Neural Networks in many Computer Vision (CV) related tasks, such as object recognition and detection, image classification and segmentation, redefining the state-of-the-art for those tasks. A CNN takes in input an image and assigns importance, in the form of weights and biases, to various aspects in the image. The main idea behind CNNs is to replace the general matrix multiplication used in Multilayer Perceptron (MLP), with the linear operator that is the convolution.

Furthermore, CNNs handle some of the problems of MLPs when working with images. In particular:

- RGB images are naturally represented as 3-dimensional vectors, or, equivalently, as a 2-dimensional matrix of pixels, in which each value is given by a tuple representing the values for each channel (red, green and blue). When dealing with MLP, images must be flattened, hence represented with a vector with a unique dimension. This representation is not able to capture all the information of an image, which resides in its spatial structure. On the other hand, since CNNs do not require to apply this transformation, they reduce the images to an easier form to process, without losing information about the spatial dependencies.

- The operation of flattening the image leads also to an increase of parameters that must be learned by an MLP. For example, a 430x430 image with 3 channels, contains 184.900 values. If we consider a single hidden layer with 1000 neurons, the number of parameters of the model would be 184.900.000. Furthermore, the increase in the number of parameters, causes the MLP model to be more prone to overfitting and with a poor convergence.
- The objective of convolution is to extract the relevant features such as edges, from the input image. Adding multiple convolutional layers, the architecture is capable to identify and extract both high-level features, giving a general understanding of the image, and low-level features, such as edges.

  Before the arrival of CNNs, the operation of transforming the image in vectors of relevant features was done with classical feature extractor techniques such as SIFT [12] and HOG [13].

A convolutional layer shifts a 2-dimensional filter, and performs a matrix multiplication between the kernel and a portion of the image, as shown in Figure 1. In mathematical terms, the convolution operator $*$ can be expressed by the formula

$$(F * k)(p) = \sum_{s+t=p} F(s)k(t)$$

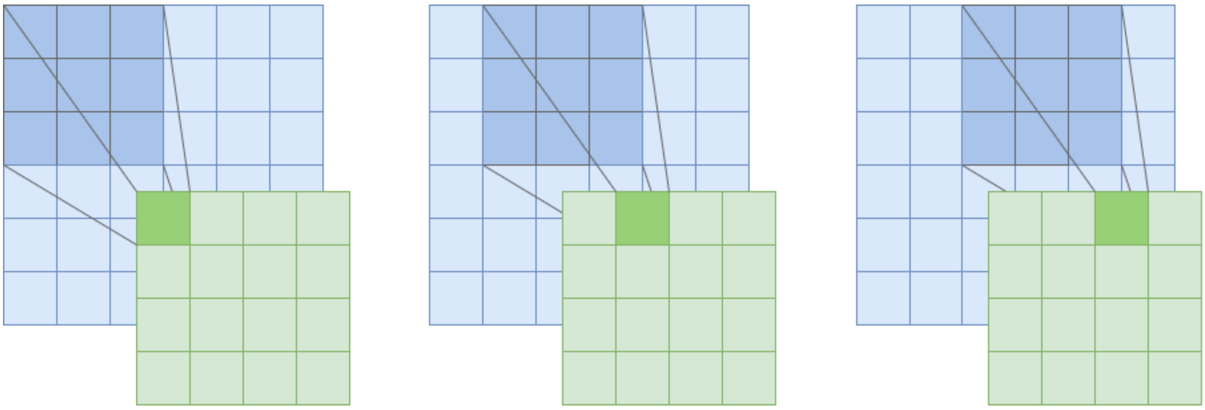

Figure 1: Example of convolution with a filter of size 3x3, stride 1 and no padding

where $F : \mathbb{Z}^2 \rightarrow \mathbb{R}$ is a discrete function and $k : [-r, r]^2 \cap \mathbb{Z}^2 \rightarrow \mathbb{R}$ is a discrete filter of size $(2r+1)^2$. A filter is a matrix of parameters which are learned by the architecture. It is relevant to notice that the dimension of the filter, hence the number of parameters, is independent of the dimension of the input.

To reduce the spatial size of the convolved features, hence reducing the computational power required to process the data, a deep convolutional architecture also includes pooling layers. These layers are also useful for extracting dominant features which are rotational and positional invariant.

2.2 ResNet

As stated in the previous paragraph, the introduction of Convolutional Neural Networks revolutionized the way of solving many tasks related to Computer Vision. The first deep convolutional architecture that produced state-of-the-art results in the task of image classification for the ImageNet competition [14] was AlexNet [15]. This architecture was built using 5 convolutional and 3 fully-connected layers. Despite the good results obtained by this architecture, a study showed that adding more layers would create a more complex function, increasing the probability of overfitting, even if some regularization techniques (such as dropout [16] or l2-norms) are applied.

The failure of adding many deep layers was mainly blamed on the vanishing/exploding gradient problem [17], which is the difficulty of updating the values of the weights in a deep architecture. In ResNet [18] the authors defined a new module for tackling the problem of the vanishing gradient, the Residual Block. A Residual Block consists of multiple layers, in which the input of the block is fed into the next layer and also added to the output of the last layer of the block (skip connection), as depicted in Figure 2. The introduction of the skip connection, allows the gradient to flow through the network.

With the introduction of residual blocks, ResNet defined the new state-of-the-art for the ImageNet classification challenge. Furthermore, the pre-trained model is nowadays widely used as a feature extractor for related tasks, or as a base for transfer learning, as described in Chapter 2.7.

2.3 Feature Pyramid Networks

Feature Pyramid Network (FPN) [19] is a feature extractor model introduced for the task of object detection and instance segmentation, to detect or segment objects at different scales in a fast and accurate way. The main idea behind this architecture is to create a pyramid of

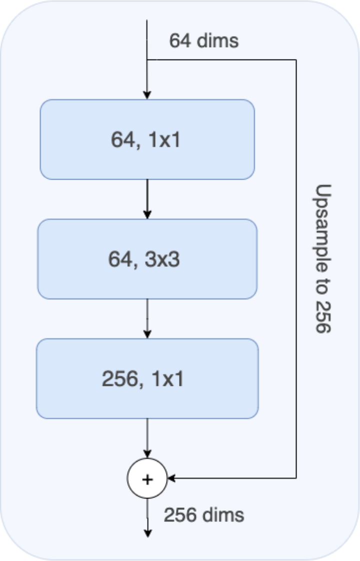

Figure 2: Residual Block introduced in ResNet

feature maps (multi-scale feature maps) which showed significant improvements compared to the regular feature maps in various tasks, such as object detection and segmentation.

FPN is composed of two paths:

- The Bottom-Up path that is a convolutional network for feature extraction, such as ResNet. Going deeper into the model decreases the spatial resolution but increases the semantic information for each layer.
- The Top-Down path is used to construct higher resolution layers from a semantic rich layer.

The bottom-up path is responsible for producing dense feature vectors at different resolutions. A dense feature vector is built using the output of a convolution module, that we call

C_i, which is used in the top-down path. In the top-down path, the i-th layer takes as input the sum of C_i (convolved with a 1×1 convolution filter) and the output of the previous layer in the path, upsampled by 2. The output of the different layers in the top-down path is also the output of the architecture.

A similar architecture is the Panoptic Feature Pyramid Network [20]. The only difference is in the top-down path. In particular, the outputs of the convolution module are convolved with a 2×2 convolution filter and upsampled by 2 until it reaches 1/4 scale. At this point, the top-down path consists of the element-wise summation of the new feature maps. Figure 3 and Figure 4 show an example of the two architectures.

2.4 Region of Interest Pooling

The Region of Interest (RoI) Pooling layer was first introduced in [21] to solve the burden of dealing with bounding boxes of different sizes in the task of object detection. This layer produces a fixed-sized feature map from inputs with different sizes, applying max-pooling on the inputs.

A RoI pooling layer takes two inputs:

- A feature map obtained from a Convolutional Model
- N bounding box (BB) coordinates representing the 'regions of interest' in the image, usually generated by a Region Proposal network.

For each bounding box, the RoI pooling layer crop the values of the input feature-map related to that region and convert the cropped section to a fixed-sized feature map. The most

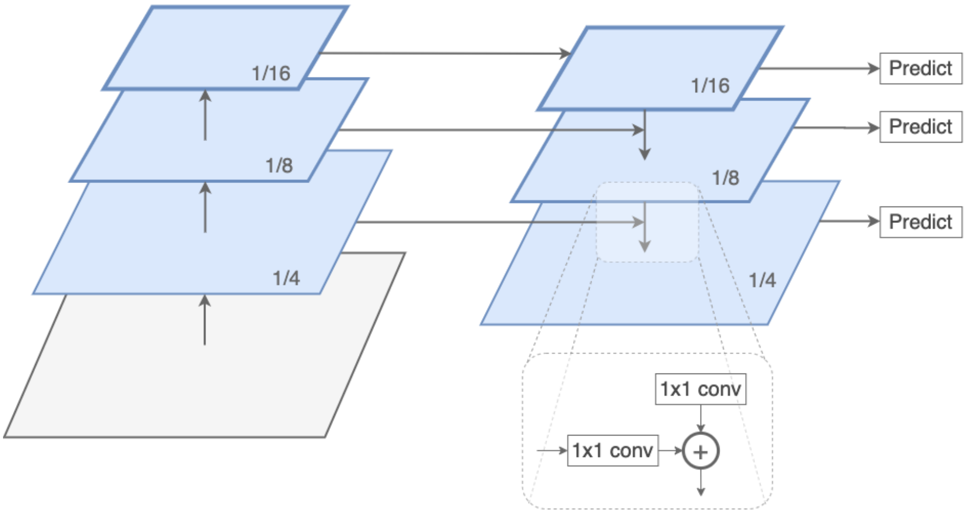

Figure 3: Feature Pyramid Network

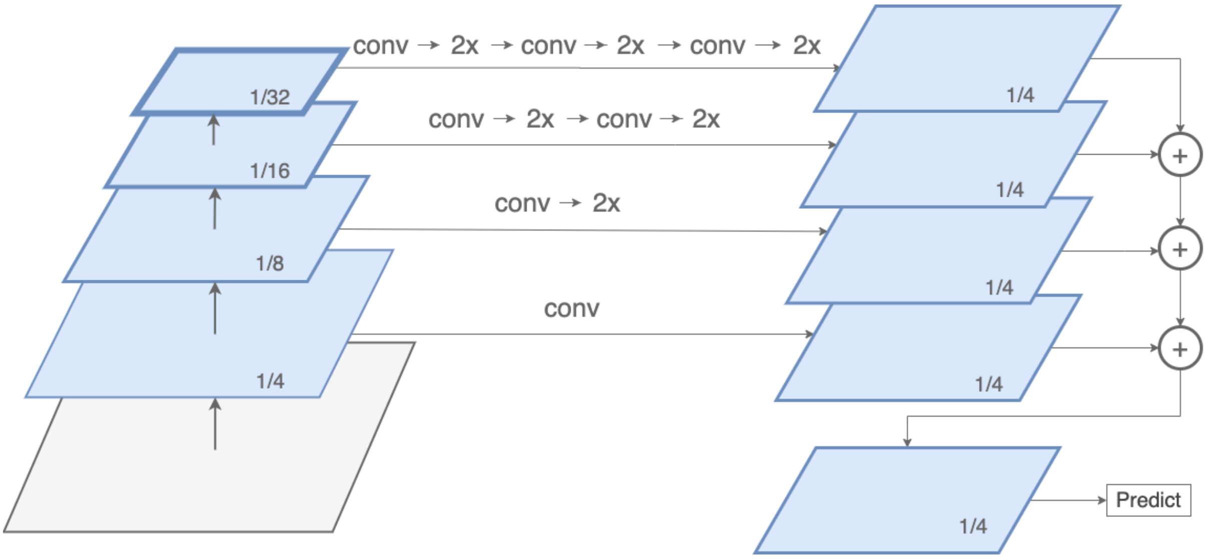

Figure 4: Panoptic Feature Pyramid Network

important feature of this layer is its capability of producing a fixed-size representation. The size of the new representation is a parameter of the layer itself, hence it is independent both from the dimension of the input feature map and from the RoI size.

Another parameter required by the RoI layer is the spatial scale. In a region proposal network, the RoIs are generated based on the input image size. Hence, there is a need to rescale them to extract the relevant region from the input feature map. For example, with an input image of size 160×160 and a feature map of size 20×20, the spatial scale parameter value is 0.125.

The operations carried out by the RoI pooling layer can be summarized as:

- The rescaling phase, which consists of dividing each BB coordinate by k (the spatial scale parameter) and take the integer part, obtaining the new coordinates relative to the input feature map.
- The operation of quantization, in which the cropped part of the feature map is divided into bins, resulting in a $n \times n$ grid, and from each bin, the maximum or average value is extracted. This results in a fixed-sized feature map relative to the RoI.

Figure 5 shows the process of applying RoI pooling for a single RoI.

An alternative to the RoI Pooling layer is the RoI Align layer [22]. This last method rescales the bounding boxes more accurately with the following process

- The rescaling phase, that divides each BB coordinate by k, without rounding up

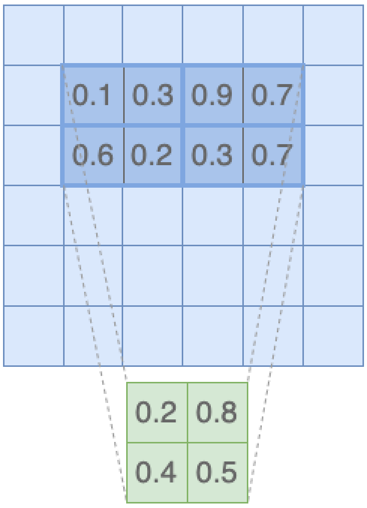

Figure 5: Example of RoI Pooling

- The quantization, in which the cropped feature map is divided into bins. For each bin are selected 4 points using bilinear interpolation, then the maximum or average value is extracted from these 4 points.

RoI Align is usually preferred to RoI Pooling when dealing with image segmentation because it does not introduce the misalignment between the RoI and the extracted features.

2.5 Face Alignment

Face alignment, also known as face normalization, is the process of identifying landmarks in images containing human faces, and to use those landmarks to obtain a new face image such that the eyes are aligned and the face is centered. This result is accomplished through scaling, rotating, and translating the input image.

Face alignment has been proved to be beneficial for the tasks of face recognition and expression recognition [23] because reduces the variations in face scale and in-plane rotations [24]. Two main types of face alignment exist:

- **3D-alignment** defines a 3D reference landmark model, and transform the input image in such a way that the landmarks of the input image match the landmarks in the 3D model
- **2D-alignment**, is a simpler alignment method that relies on the scale, rotation and translation of the input image based on the detected facial landmarks

The process of the 2D face alignment can be summarized as:

- **Face detection and Landmark Localization**, which consists of determining the location of the face (or faces) in the input image and to extract localized landmark coordinates (usually 5, 44 or 64). Classical face detection algorithms are Haar Cascades Classifier [25] or Histogram of Oriented Gradients (HOG) [13].

  A widely used DNN based face and landmark detection model is Multi-Task CNN (MTCNN) [26] which employs multi-task learning and a cascade of learners to detect facial landmarks.
- **Image warping and transformation** is the last phase, and consists of warping and transforming the input image to an output coordinate space, given a set of facial landmarks.

  There are different types of transformations that can be applied in this phase. In our work,

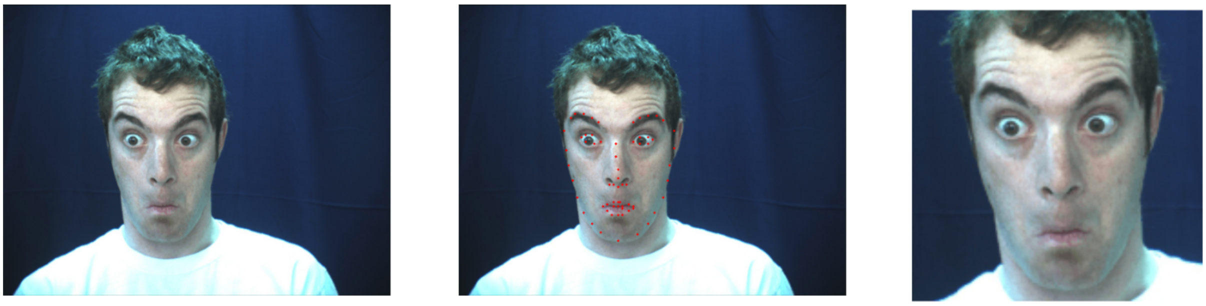

Figure 6: Landmark detection and alignment process

we will use the similarity transform [27] which is a composition of rotation, translations, and magnifications. The points in the new image are defined by the formulas

$$X = s * x * \cos(rotation) - s * y * \sin(rotation) + a_1$$

$$Y = s * x * \sin(rotation) + s * y * \cos(rotation) + b_1$$

in which s is the scale factor, x and y are the translation parameters, rotation is the angle in counter-clockwise as radians and the homogeneous transformation matrix is defined as

$$\begin{bmatrix} a_0 & b_0 & a_1 \\ b_0 & a_0 & b_1 \\ 0 & 0 & 1 \end{bmatrix}$$

Figure 6 shows an example of the alignment process.

2.6 Optimization

Optimization is one of the core components of Machine Learning. ML algorithms aim at building an optimization model that is capable of learning the parameters in the objective function from the data. The classic optimization method for DNNs is Stochastic Gradient Descent (SGD) [28] and its variants, with the backpropagation algorithm. SGD is a first-order optimization method that iteratively travels down the slopes of the objective function until a minimum is reached. At the end of an iteration of SGD, the backprop algorithm is used to propagate the gradient updates in the network.

With Vanilla SGD, however, it is easy to fall in local minima or saddle point, often present in the objective function. For this reason, momentum is usually added to SGD. Momentum [29] is used to accumulate the gradients of the past steps, which will be used to determine the weights' update for the current step. This has been proved to increase the convergency speed and to partially solve the problem of the optimization algorithm being stuck. The quantity of gradient to inject in the network is regulated by the learning rate (LR), which determines the step size of each iteration. A small value of the LR could lead to slow convergence while a high LR may not lead to convergence at all.

Some recent methods introduced the capability of adapting the learning rate based on some statistics. For example, RMSProp [30] stores the moving average of the square of the previous gradients and divides the learning rate by the root of the mean square. This allows keeping learning even if the value of the gradients is very small. Another widely used optimization algorithm is Adam [31]. This method combines momentum and RMSProp and has been proved to provide good performances for a wider range of learning rates.

2.7 Transfer Learning

Transfer Learning [32] is a widely used machine learning technique where a model which has been trained on a task can be used as a starting point for a similar task. There are several reasons why this technique has become popular and widely used

- **Data requirement**: DL models usually require a huge amount of high-quality annotated data, which is not often available. With transfer learning, the model may be fine-tuned in a smaller dataset producing high-quality results.
- **Computation**: DL techniques are known to be computationally intensive. With transfer learning, we can save hours of computations without incurring in a decay of the results.
- **Overfitting**: The high number of parameters in a DL model can lead to an increase in variance which leads to a low generalization capability. This problem can be leveraged relying upon information from a related domain. z
- **Model features**: Some of the features learned by a DL model can be transferred to another domain without relevant modifications.

CHAPTER 3

PREVIOUS WORK

In this chapter, we present some of the current works in AU detection which we have taken as inspiration to develop our model. In recent years, Deep Learning approaches have dominated the scene on multiple CV tasks. In Facial Action Unit detection, the first Deep Learning based work that achieved considerable results, was developed in 2014. Since then, most of the works are based on deep neural networks.

3.1 Deep Region and Multi-label Learning for Facial Action Unit Detection

Deep Region and Multi-Label Learning (DRML) [33] is one of the first Convolutional Neural Network based model for AU recognition. The authors address two main problems in AU recognition:

- **Region Learning (RL)** identify the sparse facial regions in which the AUs are active, to improve detection performance. A particular example of RL is Patch Learning, which consists of dividing the face image into uniform patches and train a model to assign a value of importance to each patch.
- **Multi-Label Learning (ML)** is a consequence of the strong correlation between some AUs. Previous works on AU detection extracts the correlation information from either FACS heuristics or ground truth labels and uses them as input to the model. On the other

hand, the authors enforce the model to learn those correlations without prior knowledge of the correlation between AUs.

The main component introduced in the model is the region layer, whose main function is to identify the patches considered relevant for detecting the AUs. The region layer takes as input the feature map produced by the first convolutional layer and divides into 8×8 patches. Each patch is fed into a second convolutional layer and then summed to the original patch. The new re-weighted patches are then concatenated, resulting in a weighted feature map of the same size as the input. The use of the region layer shows an improvement in identifying AU discriminative regions compared to a standard CNN, such as AlexNet or ConvNet.

3.2 EAC-Net: Deep Nets with Enhancing and Cropping for Facial Action Unit Detection

The Enhancing And Cropping (EAC) network [34], is based on a VGG [35] network, in which the following layers are also added:

- **Enhancing Layers** are attention layers whose aim is to give more importance to the regions of the image that are associated with the AUs. This attention layer is implemented as a special type of skip connection between the input and the output of two groups of convolution in the backbone model.

  In detail, the output feature map of a group of convolutions is multiplied element-wise by a handcrafted attention map and in parallel processed by the convolutional layers of the next group. The two output feature maps are then fused by element-wise summation.

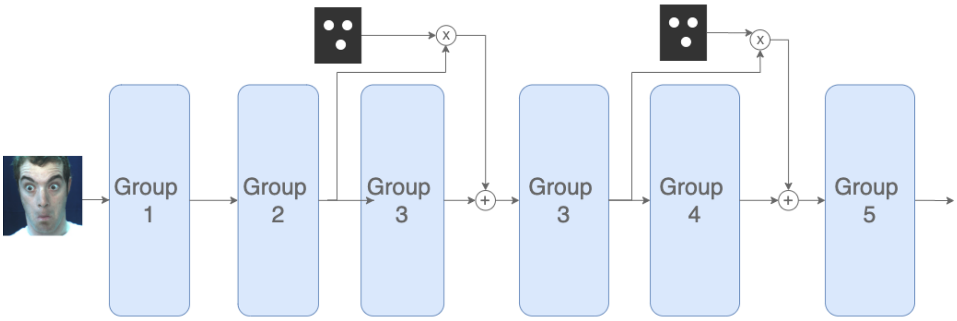

Figure 7: High-levek overview of the backbone model with Enhancing Layers

This process is repeated for two consecutive groups of convolutional layers. Figure 7 gives a high-level overview of this module.

- **Cropping layers** are used to learn features for specific AUs. This module is composed of 20 branches in which each branch takes as input the cropped part of the output feature map of the enhanced VGG. The cropped region is the rescaled center of the 20 AU centers used in the attention map of the enhancing layers.

  Each branch upsamples the cropped feature map which is then fed into a convolutional layer. The outputs of the convolutional layers are concatenated and processed by a FC network to produce the final prediction.

In subsequent work, the author included temporal information to the network, adding two LSTM layers at the end of the previous model, before the dense layer used for the prediction. EAC and EAC with LSTM achieved good results compared to previous works on AU detection, particularly when the temporal information is introduced in the network.

3.3 Joint Facial Action Unit Detection and Face Alignment

In Deep Adaptive Attention for Joint Facial Action Unit Detection and Face Alignment [36], the authors defined a deep neural network (JAA-Net) that jointly estimates AUs and facial landmarks (face alignment). JAA-Net consists of the following modules:

- **Hierarchical and multi-scale region learning** is used to extract features at different scales. Similarly to DRML [33], this layer aims at sharing the filter weights within patches with different weights assigned to each patch.

  This module is composed of an input layer and three hierarchical convolutional layers. The multi-scale version stands for how the input of a convolution layer is modeled. In particular, the intermediate 8×8, 4×4, and 2×2 patches of the second, third and fourth convolutional layers are the result of convolution on corresponding patches in the previous layer, input, first and second, respectively. The outputs of the three intermediate layers are concatenated, and the final result is summed element-wise with the output of the input layer. In Figure 8 is shown the structure of the hierarchical and multi-scale module.

- **Face alignment** estimates the locations of facial landmarks and generates the initial attention maps that will be used in the next module. This module includes three convolutional layers and a fully connected layer with 2 hidden layers.

- **Adaptive attention learning** is used to refine the initial AUs' attention maps and consists of two steps:

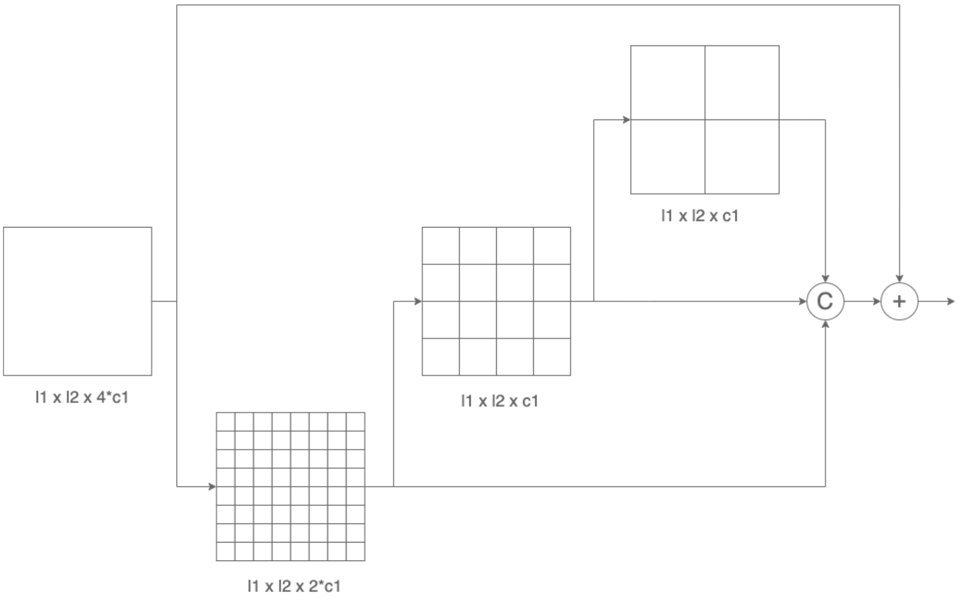

Figure 8: Hierarchical and Multi-Scale module in [36]. In the figure, $l_1 \times l_2 \times c_1$ represent the height, width, and channels of one layer, respectively

- **AU attention refinement** takes as input the handcrafted RoIs for each AU similarly to EAC-Net [34], and applies a series of convolution to the RoI masks using different branches. The output of each branch is multiplied element-wise with the feature maps of the hierarchical region learning.
- **Local AU Feature Learning** is composed of a series of convolutions and pooling layers. This module takes in input the refined AUs from each branch, and outputs a new AU attention map, applying element-wise summation over each convolutional branch.

To estimate probabilities of the AUs occurrences, the output feature maps of the face alignment and the hierarchical and multi-scale region learning are concatenated together and fed into a FC network with two hidden layers.

3.4 Facial Action Unit Detection Using Attention and Relation Learning

In Facial Action Unit Detection Using Attention and Relation Learning [37], the authors defined a deep learning framework (ARL) based on attention and relation learning for AU detection. ARL is composed of 4 modules:

- **Hierarchical and Multi-Scale region learning**, as defined in JAA-Net [36].
- **Channel-Wise Learning** consists of a multi-branch architecture whose aim is to select AU related features. For each action unit, the output of the region learning is fed into a convolutional layer and pooled. This process produces a vector of channel-wise attention weights. This vector is multiplied with the output of the convolution, obtaining a channel-wise weighted feature.
- **Spatial Attention learning** which takes as input the channel-wise weighted feature and process it with a convolutional layer, obtaining a spatial pixel-wise feature map. The feature map is convolved with a single-channel convolutional layer and a sigmoid function is applied, obtaining an initial spatial attention weight.
- **Pixel-Level Relation Learning** module captures the dependencies at pixel-level used to refine spatial pixel-wise attentions. This module consists of a Conditional Random Field [38] which takes as input the spatial attention weight and the convolved output

of the Channel-Wise learning module, obtaining a refined spatial attention weight. The result is then multiplied with a new convolved version of the output of the Channel-Wise module.

Finally, the output of the Pixel-Level Relation learning module is processed by a FC module to predict the AUs' occurrence.

CHAPTER 4

MODEL STRUCTURE

In this chapter, we give an in-depth description of the proposed architecture. In particular, we explain the face alignment and Region of Interest extraction processes. Then, we describe the Feature Pyramid Network and how this has been integrated with the Region of Interest pooling module to solve the problem of AU detection.

4.1 Model Overview

As depicted in Figure 10, our architecture is composed of two main branches: the first one consists of creating an aligned representation of the input image, which is then fed into the Feature Pyramid Network that produces the encoding of the image, as detailed in Section 4.2. We choose to use this structure because of its capability of extracting global features at different scales, which has been proved to be beneficial for detecting AUs [36; 37]. The features extracted by the FPN are fed into the Region of Interest module.

The second branch generates the bounding boxes for the Regions of Interest, which in this case consists of regions of the face that are relevant to detect the different action units. The Region of interest module consists of a multi-branch architecture that processes a feature map differently based on the location of the occurrence of the AU in the face. The main purpose of this module is to extract the local features related to the pre-defined bounding boxes. More details are given in Section 4.3.

In this work, we aim at detecting 8 action units, shown in Figure 9, which are AU1, AU2, AU4, AU6, AU9, AU12, AU25, AU26. Since the reference action units are centered in different regions of the face, we choose to partition them based on the portion of the face in which they occur. In particular, we defined 3 different face regions:

- **Upper face** which contains the eyes and the forehead
- **Middle face** is composed of the cheeks and the nose
- **Lower face** includes the mouth and the chin

4.1.1 Landmark Localization and Face Alignment

The first step is the detection of 64 facial landmarks that are used to align the image and to create the bounding boxes related to the RoIs. In particular, the process of aligning the image aims at normalizing the image in terms of scale and rotation, such that the position of the eyes does not change in all the images of the datasets.

The facial landmarks are computed using the neural network based model described in [41] and available in PyTorch [42]. This model is capable of providing reliable landmarks also in case of partial occlusion of the face. After retrieving the facial landmarks, we align the image using similarity transformation, as previously described in Section 2.5.

The identified landmarks, together with 64 reference landmark positions, are used to estimate the transformation matrix which is applied to the input image. The result consists of the cropped, rotated, and resized input image, with a fixed size of 160 × 160 pixels. Figure 11 shows the process of landmark localization and alignment.

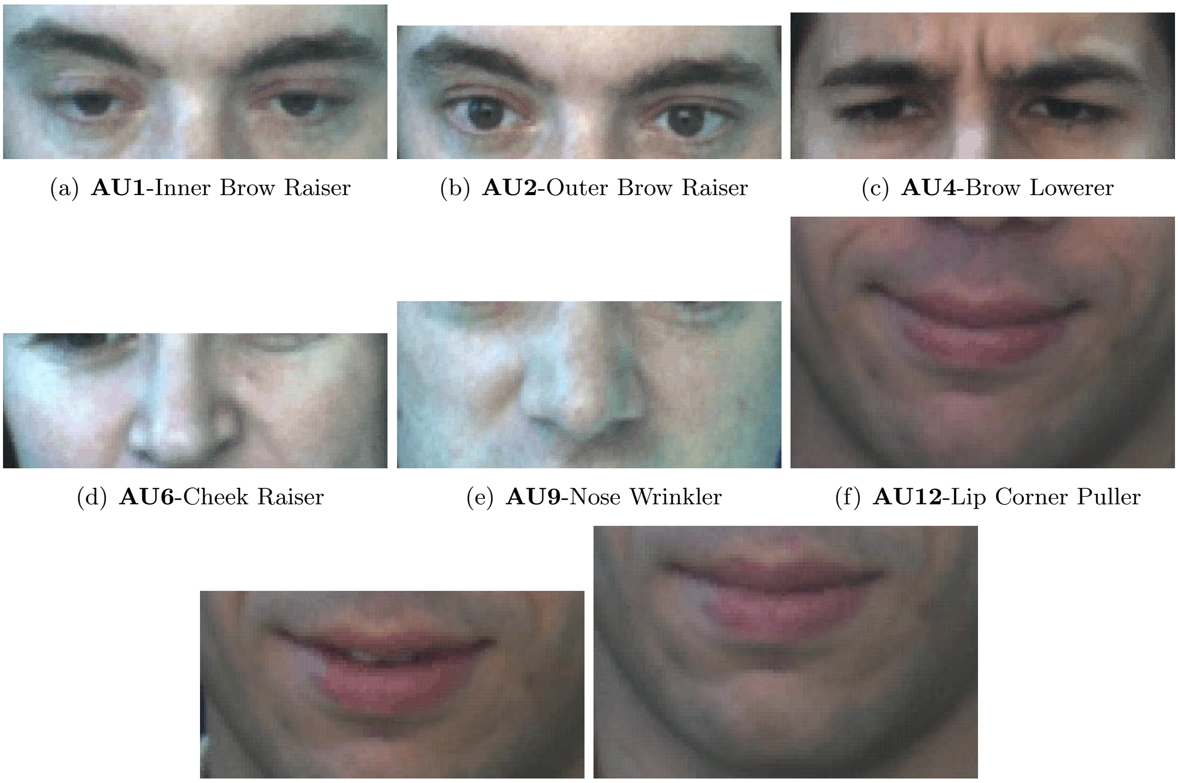

(a) **AU1**-Inner Brow Raiser

(b) **AU2**-Outer Brow Raiser

(c) **AU4**-Brow Lowerer

(d) **AU6**-Cheek Raiser

(e) **AU9**-Nose Wrinkler

(f) **AU12**-Lip Corner Puller

(g) **AU25**-Lips Part

(h) **AU26**-Jaw Drop

Figure 9: Examples of the AUs in DISFA [39; 40]

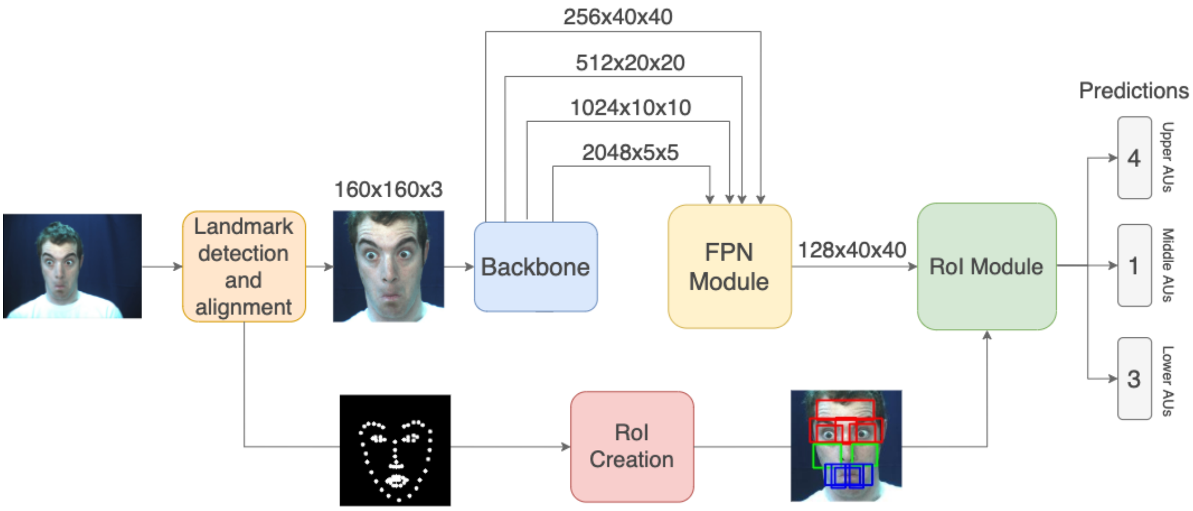

Figure 10: Overview of the complete architecture

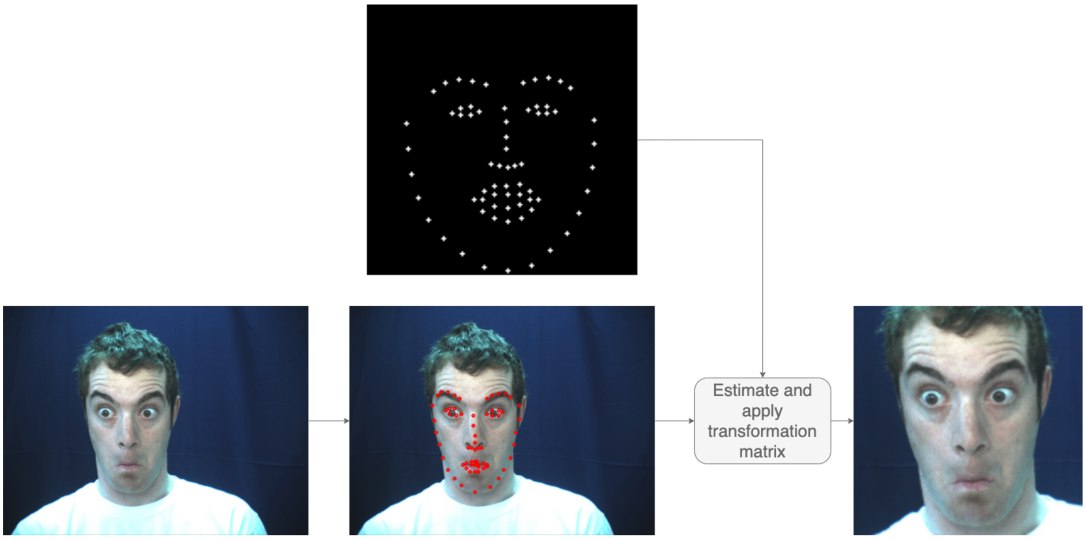

Figure 11: Landmark localization and face alignment process

Face portion	AUs	Number of RoIs
Upper	1, 2, 4, 6	5
Middle	9	2
Lower	12, 25, 26	4

TABLE II: Regions of Interests and face portion

4.1.2 Creation of the Regions of Interest

To determine the Regions of Interests, we first define the locations of the centers of the AUs. Subsequently, we guide the creation of the bounding boxes related to the RoIs based on the facial landmarks detected as described in the previous section.

More in detail, we defined a variable number of RoIs for each part of the face, as detailed in Table II. Since we are extracting the bounding boxes taking into consideration the relative position of the AU centers' with respect to multiple facial landmarks, the bounding boxes are dynamically defined and adapted to the face. Figure 12 shows the RoIs extracted for a single image.

4.2 Feature Pyramid Network Module

The encoder portion of our architecture is inspired by the Panoptic Feature Pyramid Network described in Section 2.3, and it is used to extract features at different resolutions. The input of this network is an RGB image of size $160 \times 160 \times 3$. The bottom-up path, which is the backbone of the network, consists of a ResNet-50 architecture. More in detail, this backbone is a collection of 4 groups of convolutions, preceded by a stem module composed of a 7×7 convolution and a 3 max-pooling layer, as described in the Table III.

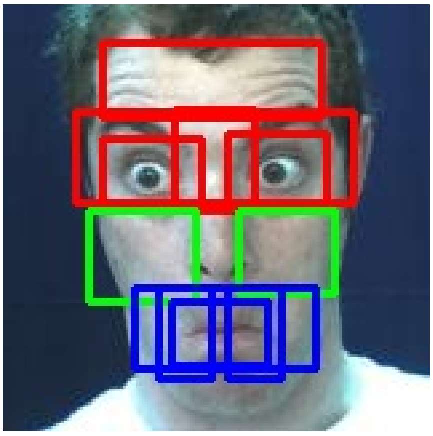

Figure 12: Example of the extracted RoIs. In red, green and blue we show the bounding boxes of the upper, middle and lower face, respectively

Layer Name	Output Size	Operations
conv1	$64 \times 1/4 \times 1/4$	$7 \times 7, 64,$ stride 2 3×3 max pool, stride 2
conv2	$256 \times 1/4 \times 1/4$	$\begin{bmatrix} 1 \times 1, 64 \\ 3 \times 3, 64 \\ 1 \times 1, 256 \end{bmatrix} \times 3$
conv3	$512 \times 1/8 \times 1/8$	$\begin{bmatrix} 1 \times 1, 128 \\ 3 \times 3, 128 \\ 1 \times 1, 512 \end{bmatrix} \times 4$
conv4	$1024 \times 1/16 \times 1/16$	$\begin{bmatrix} 1 \times 1, 256 \\ 3 \times 3, 256 \\ 1 \times 1, 1024 \end{bmatrix} \times 6$
conv5	$2048 \times 1/32 \times 1/32$	$\begin{bmatrix} 1 \times 1, 512 \\ 3 \times 3, 512 \\ 1 \times 1, 2048 \end{bmatrix} \times 3$

TABLE III: ResNet-50. The fractions 1/4, 1/8, 1/16 and 1/32 refer to the height and width ratios with respect to the input image size

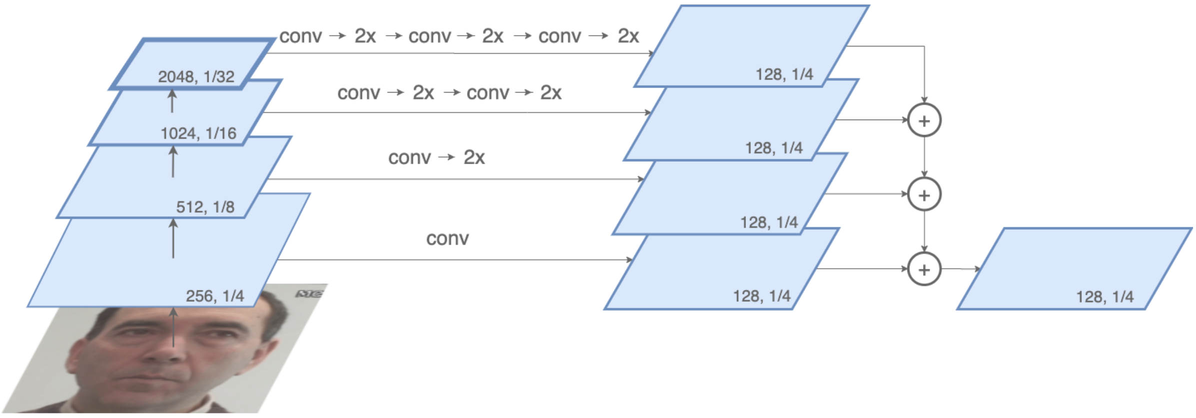

Figure 13: Feature Pyramid Network used in our architecture

In the top-down path, the output features of each group are fed into an upsampling module, composed by a 3 × 3 convolution, batch normalization, ReLu, and 2× bilinear upsampling, as it is illustrated in Figure 13. From the deepest level of the FPN (at 1/32 scale), we perform three upsampling stages to yield a feature map at 1/4 scale. This process is repeated for all the remaining feature maps, with progressively fewer upsampling stages. The upsampled features are then summed element-wise generating the output feature map with 128 channels at 1/4 scale, which will be used as input for the RoI module, as explained in Section 4.3. Figure 13, shows the details of the FPN model.

4.3 Regions of Interest Module

The RoI module is used to extract local features related to the AUs located in different regions of the face, and to estimate the presence of the AUs for that portion of the face.

Since we split the AUs based on their location of occurrence in the face, i.e., upper, middle, and lower part of the face, we define three different branches:

- **Upper Branch** extracts the local features of the AUs that occurs in the upper region of the face. Particularly, the eyes, the forehead, and between the eyebrows.
- **Middle Branch** takes into consideration the middle part of the face. We are interested in detecting the AU related to the cheeks' movement.
- **Lower Branch** is tasked with the extraction of the features for the AUs in the lower part of the face. More in detail, we defined the RoIs to extract features related to the mouth, the chin, and the corners of the lips.

Each branch takes as input the multi-scale feature map produced by the FPN module and outputs a vector of estimations for the AUs related to that branch.

A branch consists of a RoI Align layer, described in Section 2.4, that extracts the local features for each of the bounding boxes, and produces a fixed-size feature map. The output size of this layer is $\#\text{RoIs} \times 128 \times \text{pooling size} \times \text{pooling size}$. These maps are then concatenated on the second dimension and average pooling is applied, before feeding the vector feature map into the bottleneck of each branch. Each bottleneck module is composed of a FC network, with 3 hidden layers. The last layer has a Softmax activation function which generates the estimation for the AUs related to that specific branch.Figure 14 shows the details for this module.

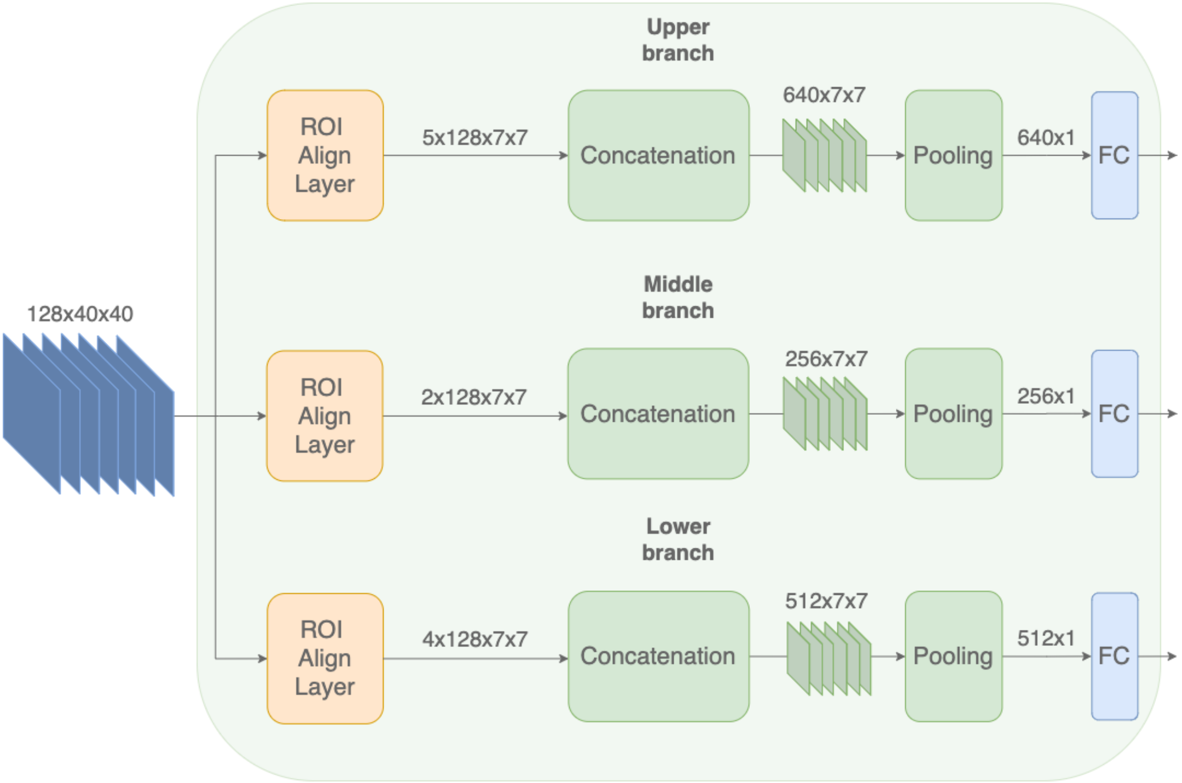

Figure 14: Overview of the Region of Interest module

CHAPTER 5

TRAINING AND VALIDATION

This chapter gives more details about the datasets that we used to train and validate the model, and the training and validation procedures applied.

5.1 Datasets

To train and validate the model, we used five different datasets:

- The **VGGFace2** [43] dataset is a face-recognition dataset with more than 3.3 million face images over more than 9,000 entities. It contains subjects with an equal gender distribution and with a variety of ethnicities and ages. The images are captured "in the wild" such that the images are exposed to head pose variations, different lighting, and occlusion conditions.
- The **Extended Cohn-Kanade (CK+)** [44; 45] dataset is one of the most well known laboratory-controlled databases for Facial Expression Recognition and AU recognition. The dataset contains 593 video sequences from 123 subjects. The duration of each sequence spans from 10 to 60 frames, and it starts from a neutral face to the peak expression. Since the AU is provided for each sequence, usually the last three frames are extracted along with the first frame (neutral expression).
- The **UNBC-McMaster shoulder pain expression** [46] database contains videos of subjects who were suffering from shoulder pain, while they were performing some actions.

This dataset contains 200 sequences from 25 subjects. Each frame has been coded by certified FACS coders, resulting in a total of around 47,000 coded frames.

- The **Compound of Facial Expression Emotions (CFEE)** [10], is a database of compound emotions images, i.e., emotions constructed by combining basic emotions. The authors defined a total of 21 compounds and basic emotions. The dataset is a collection of 230 subjects with around 21 images for each one, for a total of 4,816 FACS coded frames.
- The **DISFA** [39; 40] database, is one of the main benchmark datasets in AU recognition. It is a collection of 27 sequences, with around 4,800 FACS coded frames for each sequence, from 27 subjects. Each frame is labeled with AUs intensities ranging from 0 to 5. The 8 coded AUs are AU1, AU2, AU4, AU6, AU9, AU12, AU25, and AU26.

5.2 Training and Validation

In Section 2.7, we stated that transfer learning is a well-known method that helps the model to improve generalization and speed up convergence. In our case, we initialize the weights of the ResNet backbone with the weights obtained from training it on the VGGFace2 [43] dataset for face recognition. The weights that we used are publicly available in [47].

The second training phase aims at fine-tuning the full model for recognizing the facial action units. Each aligned image of size 160 × 160 is normalized in the same way as the pre-trained backbone with the values shown in Table IV.

At training time we also apply some data augmentation techniques, to increase and diversify the available data, and to improve the robustness of the model. We limited the augmentation to variation in color and flipping to avoid distortion of the face in the input image and to simulate

Channel	μ	σ
R	0.485	0.229
G	0.456	0.224
B	0.406	0.225

TABLE IV: Normalization values (mean and standard deviation) for each channel

events such as illumination variations and occlusions. In particular, the training dataset has been augmented using:

- **Horizontal flip** which flips the image horizontally. Since the AUs are symmetrical, flipping the image allows us to increase the amount of training data without losing information on the location of the action units
- **Color Jitter** performs random brightness, contrast, hue, and saturation variations so that the model would be more robust to these variations at inference time
- **Cutout** [48] consists of masking out a random part of the input image. This technique simulates occluded examples, encouraging the model to take into consideration a more diverse set of features for classifying images. For example, to classify a car, the model would be enforced to look at other details of the image, instead of just focusing on the wheels.

To reduce the imbalance of the training data towards neutral samples, i.e. faces without visible action units, and to increase the diversification of the data, which is reduced by the

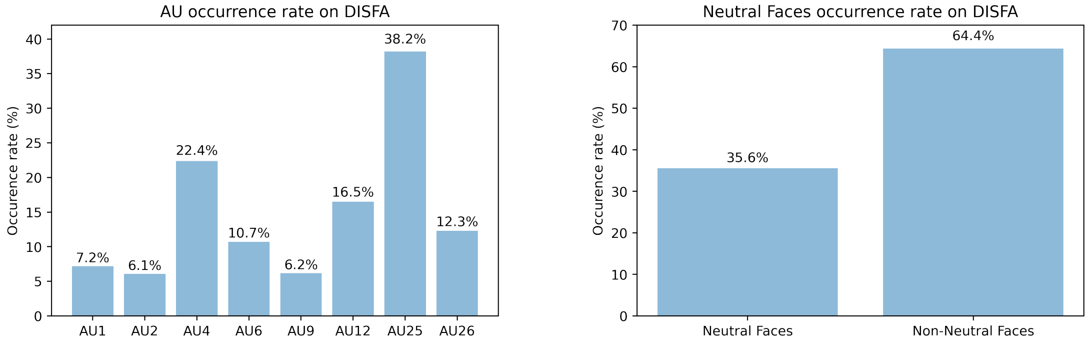

(a) Occurrence rate of Action Units

(b) Occurrence rate of Neutral Faces

Figure 15: Occurrence rates of AUs and Neutral Faces in DISFA

similarity of subsequent frames, we sub-sampled the images with neutral faces, including in the training data 1 frame over 5.

To validate the model, we performed 3-fold cross-validation on the DISFA dataset, splitting the data based on the subjects. In particular, we used the splits provided by [36]. Splitting the data based on the subjects force the model to be as much subject-independent as possible. Figure 15 shows the distribution of AUs and neutral faces on the DISFA dataset.

The training data is then composed of the images in CK+, UNBC and CFEE, and the training folds of the DISFA dataset. Figure 16 shows the AUs' and neutral faces' distributions on the training data.

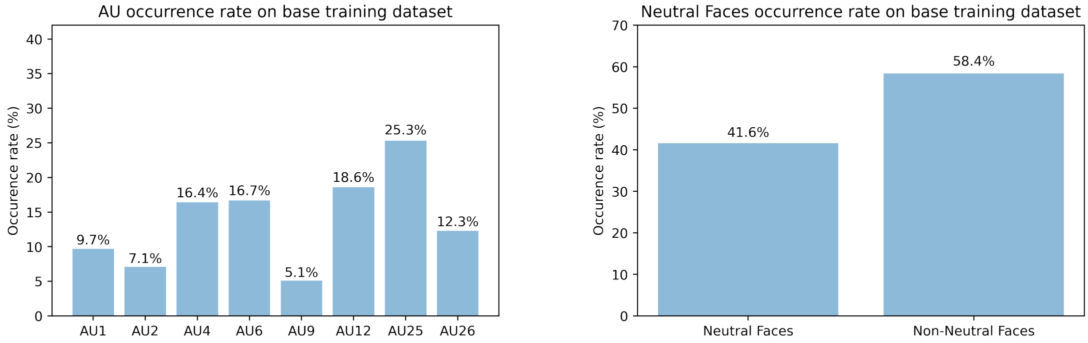

(a) Occurrence rate of Action Units

(b) Occurrence rate of Neutral Faces

Figure 16: Occurrence rates of AUs and Neutral Faces in the training data

5.3 Loss Function

Facial Action Unit detection is a multi-label classification problem because multiple AUs can occur simultaneously in an image. For this reason, we used a weighted multi-label binary cross-entropy loss function with sigmoid activation:

$$E_{BCE} = -\frac{1}{n_{au}} \sum_{i=1}^{n_{au}} w_i [p_i \log(\hat{p}_i) + (1 - p_i) \log(1 - \hat{p}_i)]$$

where

- p_i is the ground truth probability of occurrence of the i-th label (1 or 0)
- $\hat{p}_i$ represents the predicted probability of occurrence
- n_{au} is the total number of action units

- w_i is the weight introduced to alleviate the data imbalance. Particularly, we set

$$w_i = \frac{(1/r_i)n_{au}}{\sum_{i=1}^{n_{au}}(1/r_i)}$$

where r_i is the number of samples with the i-th AU in the training data

Moreover, since some AUs are rarely present in the training data, the network is biased towards absence for this AUs. To mitigate this problem, we introduce a multi-label Dice loss [49], defined as:

$$E_{Dice} = \frac{1}{n_{au}} \sum_{i=1}^{n_{au}} w_i \left(1 - \frac{2p_i\hat{p_i} + \epsilon}{p_i^2 + \hat{p_i}^2 + \epsilon}\right)$$

where ϵ is a smoothing term. The Dice coefficient is also known as the F1-score, which is the most popular metric for AU recognition, as described in Section 6. Introducing this coefficient, we take into account the consistency between the loss function and the evaluation metric while training out model.

The final loss function is

$$E = E_{BCE} + \lambda * E_{Dice}$$

where λ is an hyper-parameter used to weight the Dice loss.

The final network is trained for up to 2000 iterations in PyTorch [42], using Adam [31] to optimize the objective function. We set the initial learning rate to 10^{-4}, mini-batch size of 16, and the λ factor for the Dice Loss has been set to 1.0.

CHAPTER 6

RESULTS

In this chapter, we introduce the evaluation metrics that have been used to validate the model and we show the results and the ablation studies that we conducted.

6.1 Evaluation Metrics

- **F1-score** is the weighted average of the precision and recall. This metric is used in case of imbalanced classification problems. In this work, since we are dealing with a multi-label problem, we take into consideration the macro-averaged F1-score defined as

$$\begin{aligned} \text{F1-score} &= \frac{1}{n_{au}} \sum_{i=1}^{n_{au}} \text{F1-score}_i \\ &= \frac{1}{n_{au}} \sum_{i=1}^{n_{au}} \frac{2 * p_i * r_i}{p_i + r_i} \end{aligned} \tag{6.1}$$

  in which p_i and r_i refer to the precision and recall of the i-th class, respectively. These measures are defined as

$$\begin{aligned} \text{Precision}_i = p_i &= \frac{\text{TP}_i}{\text{TP}_i + \text{FP}_i} \\ \text{Recall}_i = r_i &= \frac{\text{TP}_i}{\text{TP}_i + \text{FN}_i} \end{aligned} \tag{6.2}$$

  where TP are the positive and correctly predicted samples, FP are the negative and correctly predicted samples and the FN are the incorrectly predicted negative samples.

- **Accuracy** is the ratio between the correct predictions and the total number of predictions. In a multi-label setting it's computed as the mean of the accuracy for the single class

  $$\begin{aligned}\text{Accuracy} &= \frac{1}{n_{au}} \sum_{i=1}^{n_{au}} \text{Accuracy}_i \\ &= \frac{1}{n_{au}} \sum_{i=1}^{n_{au}} \frac{\text{TP}_i + \text{TN}_i}{\text{TP}_i + \text{TN}_i + \text{FP}_i + \text{FN}_i}\end{aligned} \tag{6.3}$$

  where TP, FP and FN are defined above and TN represents the correctly predicted negative samples.

6.2 Results on DISFA

We compare our method against some of the SOTA AU detection works under the same 3-fold cross-validation setting. In particular, we compare against the most recent deep learning based models JAA [36] and ARL [37].

In Figure 17(a) we compare the averaged F1-score results with respect to the other methods. The chart shows that our method outperforms the others, improving the results by 5.7% and 3% with respect to JAA and ARL, respectively. For what concerns the F1-score for each single AU, Figure 17(b) shows that the AU performances are fluctuating in all the methods. A possible explanation for this behavior is that some AUs are easier to recognize with respect to others, resulting in higher F1-score performance.

In terms of accuracy score, is possible to notice in Figure 18(a) that our method achieves results analogous to the other reference methods. Even though we achieve the best accuracy on AU1, AU2, AU4 and AU6 our method preforms slightly worse in terms of accuracy in the

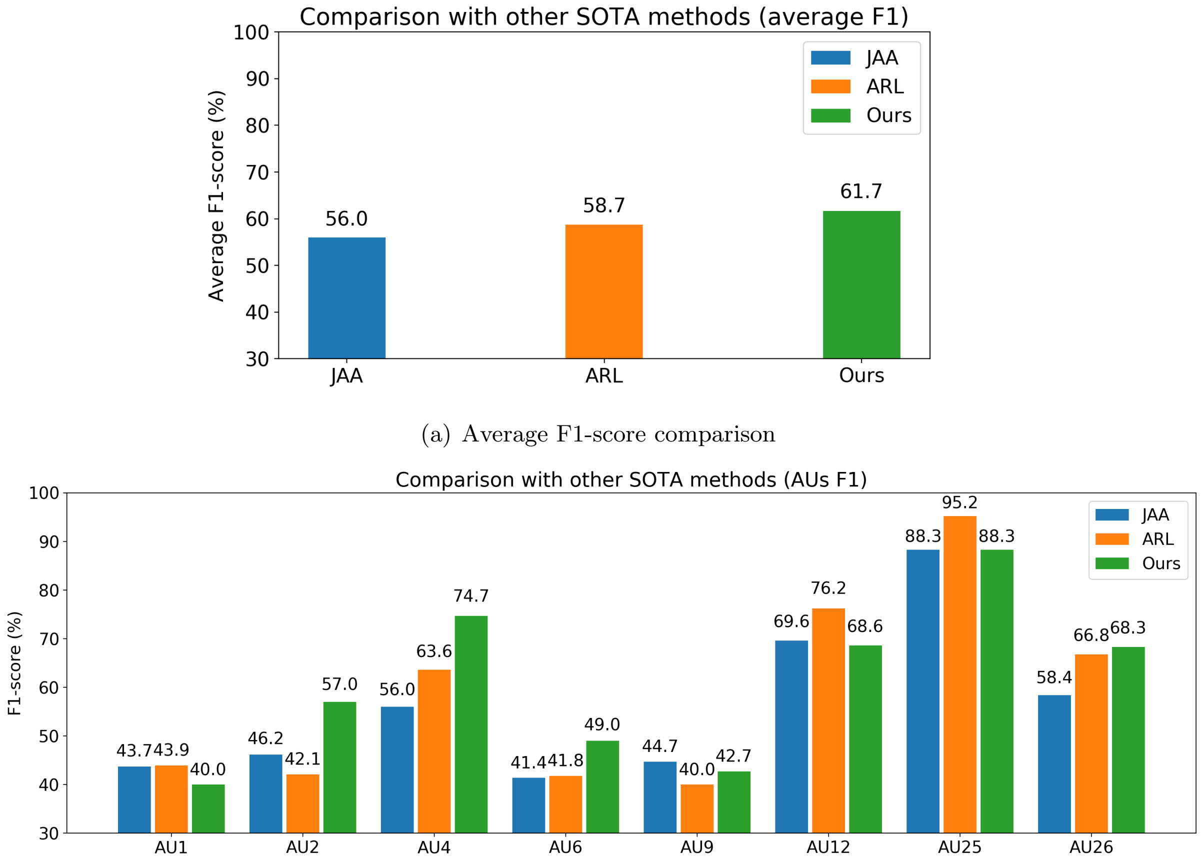

(a) Average F1-score comparison

(b) Single AU F1-score comparison

Figure 17: F1-score comparison of JAA, ARL and Our method

prediction of the AUs located in the lower part of the face, as shown in Figure 18(b). Despite this, we should notice that the accuracy score in a multi-label setting is less representative with respect to the F1-score, since it doesn't show the differences with respect to a biased model.

6.3 Ablation Studies

In this section, we conduct an analysis on the effects of various model components' and different training techniques that we applied. In Figure 19(a) we show the results obtained removing some components of the model, in particular:

- **ResNet** refers to the pure ResNet-50 model of [1]
- In **ResNet+RoI**, we removed the FPN bottleneck representation
- **FPN+RoI** is the final model with FPN and RoI

All the different models have been trained and validated with the same settings, in terms of training and validation data, hyperparameters, and validation procedure.

As we can see, the base model achieves the lowest result in terms of averaged F1-score. A more in-depth analysis showed that the images with an active AU2 (outer brow raiser) were mainly misclassified as AU1 (inner brow raiser). Including the Region of Interest pooling improves the results by almost 3%. The best results are obtained when taking into consideration the multi-scale features produced by the FPN, obtaining an increase of 6.4% and 3.5% compared to the ResNet and Resnet with RoI pooling, respectively.

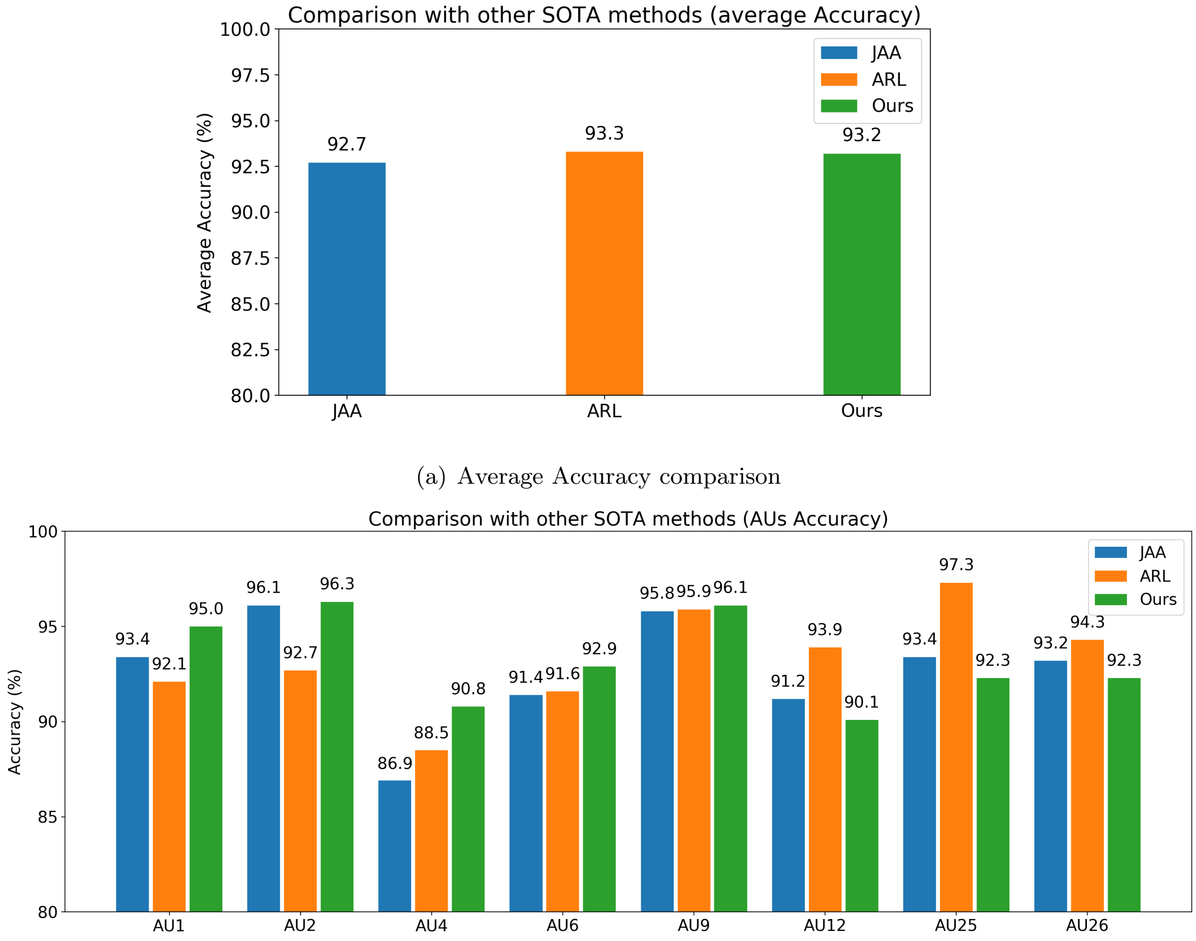

(a) Average Accuracy comparison

(b) Single AU Accuracy comparison

Figure 18: Accuracy comparison of JAA, ARL and Our method

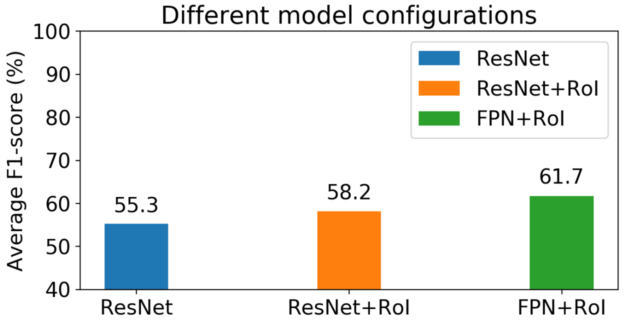

(a) Average F1-score for different model configurations

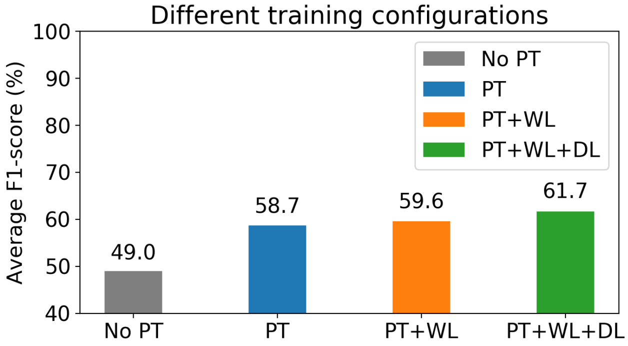

(b) Average F1-score for different training configurations

In Figure 19(b) we show the results obtained training the final model under different training settings. As we can notice, the pre-training phase of the model gives the best improvements in terms of F1-score, bringing the F1 results from 49.0% to 58.7%.

Moreover, the model trained with the weighted loss and the dice loss produces the best results. In particular, weighting the Binary Cross Entropy loss improves the prediction results by 0.9%, and the introduction of the Dice loss leads to the best results, with an increase of 2.1% in terms of F1-score.

CHAPTER 7

CONCLUSIONS AND FUTURE DIRECTIONS

In this thesis, we designed a new deep learning based architecture for Facial Action Unit detection that achieves results superior to other state-of-the-art models, in terms of F1-score. We showed that the use of a Feature Pyramid network allows the model to learn features at different scales, which has been proven to be beneficial for the task. Moreover, we defined a new RoI pooling layer that extracts specific features for different regions of the face, and contribute to the detection of AUs in a specific region in the face.

We evaluated the efficacy of our approach on the available benchmark dataset and motivated our choices through ablation studies. There are possible developments for improving the current model:

- **Increasing training data** might improve the robustness of the model, in particular for the AUs that appear less frequently. As shown in Section 6.3, with a significant amount of pre-training images the model provides better results.
- **Enclose temporal information** can be beneficial for the detection. AUs are related to the movement of some muscle, hence they can be interpreted as a mutation of the shape in a specific region of the face. Introducing temporal information would take into consideration these variations in the face.

  To do so, we can introduce an LSTM module before each FC layer on each branch, and training the model with multiple subsequent images, instead of using a simple image. This solution can be beneficial in terms of the obtained result, at the cost of longer training time.

- As an alternative to training on sequence data, the use of a Neutral face as **reference frame** might be beneficial for the model. With such an approach, the model can be trained to learn the differences in aspects between a neutral face and the one in which the AUs are occurring.
- The RoI extraction can lack precision in case of mispredicted facial landmarks, which is mostly due to high head-pose variations. In such a case the model will not be able to extract the correct face region that will be used for the AU detection. For this reason, a **manual annotation of the regions of interest made by experts** could increase the prediction accuracy of the model, but would also increase the cost related to the data collection.

CITED LITERATURE

1. Menchetti, G., Chen, Z., Wilkie, D. J., Ansari, R., Yardimci, Y., and Çetin, A. E.: Pain detection from facial videos using two-stage deep learning. In 2019 IEEE Global Conference on Signal and Information Processing (GlobalSIP), pages 1–5, Nov 2019.

2. Facial expressions of pain in lung cancer. Analgesia, 1(2), 1995.

3. Rubinow, D. R. and Post, R. M.: Impaired recognition of affect in facial expression in depressed patients. Biological Psychiatry, 31(9):947–953, 2020/03/24 1992.

4. Kapoor, A., Burleson, W., and Picard, R. W.: Automatic prediction of frustration. International Journal of Human-Computer Studies, 65(8):724 – 736, 2007.

5. Lankes, M., Riegler, S., Weiss, A., Mirlacher, T., Pirker, M., and Tscheligi, M.: Facial expressions as game input with different emotional feedback conditions. In Proceedings of the 2008 International Conference on Advances in Computer Entertainment Technology, ACE '08, page 253–256, New York, NY, USA, 2008. Association for Computing Machinery.

6. EKMAN, P.: Facial action coding system. 1977.

7. Lucey, P., Cohn, J. F., Prkachin, K. M., Solomon, P. E., and Matthews, I.: Painful data: The unbc-mcmaster shoulder pain expression archive database. In Face and Gesture 2011, pages 57–64, 2011.

8. Pantic, M., Valstar, M. F., Rademaker, R., and Maat, L.: Web-based database for facial expression analysis. In Proceedings of IEEE Int'l Conf. Multimedia and Expo (ICME'05), pages 317–321, Amsterdam, The Netherlands, July 2005.

9. Lucey, P., Cohn, J. F., Kanade, T., Saragih, J., Ambadar, Z., and Matthews, I.: The extended cohn-kanade dataset (ck+): A complete dataset for action unit and emotion-specified expression. In 2010 IEEE Computer Society Conference on Computer Vision and Pattern Recognition - Workshops, pages 94–101, 2010.

CITED LITERATURE (continued)

10. Du, S., Tao, Y., and Martinez, A. M.: Compound facial expressions of emotion. Proceedings of the National Academy of Sciences, 111(15):E1454–E1462, 2014.

11. LeCun, Y., Haffner, P., Bottou, L., and Bengio, Y.: Object recognition with gradient-based learning. In Shape, Contour and Grouping in Computer Vision, volume 1681 of Lecture Notes in Computer Science (including subseries Lecture Notes in Artificial Intelligence and Lecture Notes in Bioinformatics), pages 319–345. Springer Verlag, 1999. International Workshop on Shape, Contour and Grouping in Computer Vision ; Conference date: 26-05-1998 Through 29-05-1998.

12. Lowe, D. G.: Distinctive image features from scale-invariant keypoints. Int. J. Comput. Vision, 60(2):91–110, November 2004.

13. Dalal, N. and Triggs, B.: Histograms of oriented gradients for human detection. Computer Vision and Pattern Recognition, 2005. CVPR 2005. IEEE Computer Society Conference on, 1:886–893, 2005.

14. Deng, J., Dong, W., Socher, R., Li, L.-J., Li, K., and Fei-Fei, L.: ImageNet: A Large-Scale Hierarchical Image Database. In CVPR09, 2009.

15. Krizhevsky, A., Sutskever, I., and Hinton, G. E.: Imagenet classification with deep convolutional neural networks. In Advances in Neural Information Processing Systems 25, eds. F. Pereira, C. J. C. Burges, L. Bottou, and K. Q. Weinberger, pages 1097–1105. Curran Associates, Inc., 2012.

16. Srivastava, N., Hinton, G., Krizhevsky, A., Sutskever, I., and Salakhutdinov, R.: Dropout: A simple way to prevent neural networks from overfitting. J. Mach. Learn. Res., 15(1):1929–1958, January 2014.

17. Hochreiter, S.: The vanishing gradient problem during learning recurrent neural nets and problem solutions. International Journal of Uncertainty, Fuzziness and Knowledge-Based Systems, 6(2):107–116, 1998.

18. He, K., Zhang, X., Ren, S., and Sun, J.: Deep residual learning for image recognition. In 2016 IEEE Conference on Computer Vision and Pattern Recognition (CVPR), pages 770–778, 2016.

19. Lin, T., Dollár, P., Girshick, R., He, K., Hariharan, B., and Belongie, S.: Feature pyramid networks for object detection. In 2017 IEEE Conference on Computer Vision and Pattern Recognition (CVPR), pages 936–944, 2017.

CITED LITERATURE (continued)

20. Kirillov, A., Girshick, R., He, K., and Dollár, P.: Panoptic feature pyramid networks. In 2019 IEEE/CVF Conference on Computer Vision and Pattern Recognition (CVPR), pages 6392–6401, 2019.

21. Girshick, R.: Fast r-cnn. In Proceedings of the 2015 IEEE International Conference on Computer Vision (ICCV), ICCV '15, page 1440–1448, USA, 2015. IEEE Computer Society.

22. He, K., Gkioxari, G., Dollár, P., and Girshick, R.: Mask r-cnn. In 2017 IEEE International Conference on Computer Vision (ICCV), pages 2980–2988, 2017.

23. Mollahosseini, A., Chan, D., and Mahoor, M. H.: Going deeper in facial expression recognition using deep neural networks. In 2016 IEEE Winter Conference on Applications of Computer Vision (WACV), pages 1–10, 2016.

24. Li, S. and Deng, W.: Deep facial expression recognition: A survey. IEEE Transactions on Affective Computing, PP, 04 2018.

25. Viola, P. and Jones, M.: Rapid object detection using a boosted cascade of simple features. In Proceedings of the 2001 IEEE Computer Society Conference on Computer Vision and Pattern Recognition. CVPR 2001, volume 1, pages I–I, 2001.

26. Zhang, K., Zhang, Z., Li, Z., and Qiao, Y.: Joint face detection and alignment using multitask cascaded convolutional networks. IEEE Signal Processing Letters, 23(10):1499–1503, 2016.

27. Anonymous: Affine transform. https://scikit-image.org/docs/dev/api/skimage.transform.html#skimage.transform.AffineTransform, 2018.

28. Rumelhart, D. E., Hinton, G. E., and Williams, R. J.: Learning Representations by Back-propagating Errors. Nature, 323(6088):533–536, 1986.

29. Sutskever, I., Martens, J., Dahl, G., and Hinton, G.: On the importance of initialization and momentum in deep learning. In Proceedings of the 30th International Conference on Machine Learning, eds. S. Dasgupta and D. McAllester, volume 28 of Proceedings of Machine Learning Research, pages 1139–1147, Atlanta, Georgia, USA, 17–19 Jun 2013. PMLR.

CITED LITERATURE (continued)

30. Tieleman, T. and Hinton, G.: Lecture 6.5—RmsProp: Divide the gradient by a running average of its recent magnitude. COURSERA: Neural Networks for Machine Learning, 2012.

31. Kingma, D. P. and Ba, J.: Adam: A method for stochastic optimization, 2014. cite arxiv:1412.6980Comment: Published as a conference paper at the 3rd International Conference for Learning Representations, San Diego, 2015.

32. Tan, C., Sun, F., Kong, T., Zhang, W., Yang, C., and Liu, C.: A Survey on Deep Transfer Learning: 27th International Conference on Artificial Neural Networks, Rhodes, Greece, October 4–7, 2018, Proceedings, Part III, pages 270–279. 10 2018.

33. Zhao, K., Chu, W.-S., and Zhang, H.: Deep region and multi-label learning for facial action unit detection. In The IEEE Conference on Computer Vision and Pattern Recognition (CVPR), June 2016.

34. Li, W., Abtahi, F., Zhu, Z., and Yin, L.: Eac-net: Deep nets with enhancing and cropping for facial action unit detection. IEEE Transactions on Pattern Analysis and Machine Intelligence, 40(11):2583–2596, 2018.

35. Simonyan, K. and Zisserman, A.: Very deep convolutional networks for large-scale image recognition. In International Conference on Learning Representations, 2015.

36. Shao, Z., Liu, Z., Cai, J., and Ma, L.: Deep adaptive attention for joint facial action unit detection and face alignment. In European Conference on Computer Vision, pages 725–740. Springer, 2018.

37. Shao, Z., Liu, Z., Cai, J., Wu, Y., and Ma, L.: Facial action unit detection using attention and relation learning. IEEE Transactions on Affective Computing, PP:1–1, 10 2019.

38. Lafferty, J. D., McCallum, A., and Pereira, F. C. N.: Conditional random fields: Probabilistic models for segmenting and labeling sequence data. In Proceedings of the Eighteenth International Conference on Machine Learning, ICML '01, pages 282–289, San Francisco, CA, USA, 2001. Morgan Kaufmann Publishers Inc.

39. Mavadati, S. M., Mahoor, M. H., Bartlett, K., Trinh, P., and Cohn, J. F.: Disfa: A spontaneous facial action intensity database. IEEE Transactions on Affective Computing, 4(2):151–160, 2013.

CITED LITERATURE (continued)

40. Mavadati, S. M., Mahoor, M. H., Bartlett, K., and Trinh, P.: Automatic detection of non-posed facial action units. In 2012 19th IEEE International Conference on Image Processing, pages 1817–1820, 2012.

41. Bulat, A. and Tzimiropoulos, G.: How far are we from solving the 2d & 3d face alignment problem? (and a dataset of 230,000 3d facial landmarks). In International Conference on Computer Vision, 2017.

42. Paszke, A., Gross, S., Massa, F., Lerer, A., Bradbury, J., Chanan, G., Killeen, T., Lin, Z., Gimelshein, N., Antiga, L., Desmaison, A., Kopf, A., Yang, E., DeVito, Z., Raison, M., Tejani, A., Chilamkurthy, S., Steiner, B., Fang, L., Bai, J., and Chintala, S.: Pytorch: An imperative style, high-performance deep learning library. In Advances in Neural Information Processing Systems 32, eds. H. Wallach, H. Larochelle, A. Beygelzimer, F. d'Alché-Buc, E. Fox, and R. Garnett, pages 8024–8035. Curran Associates, Inc., 2019.

43. Cao, Q., Shen, L., Xie, W., Parkhi, O. M., and Zisserman, A.: Vggface2: A dataset for recognising faces across pose and age. In International Conference on Automatic Face and Gesture Recognition, 2018.

44. Kanade, T., Cohn, J. F., and Yingli Tian: Comprehensive database for facial expression analysis. In Proceedings Fourth IEEE International Conference on Automatic Face and Gesture Recognition (Cat. No. PR00580), pages 46–53, 2000.

45. Lucey, P., Cohn, J., Kanade, T., Saragih, J., Ambadar, Z., and Matthews, I.: The extended cohn-kanade dataset (ck+): A complete dataset for action unit and emotion-specified expression. pages 94 – 101, 07 2010.

46. Lucey, P., Cohn, J. F., Prkachin, K. M., Solomon, P. E., Chew, S., and Matthews, I.: Painful monitoring: Automatic pain monitoring using the unbc-mcmaster shoulder pain expression archive database. Image and Vision Computing, 30(3):197 – 205, 2012. Best of Automatic Face and Gesture Recognition 2011.

47. Anonymous: Pytorch face recognizer based on 'vggface2: A dataset for recognising faces across pose and age. `https://github.com/cydonia999/VGGFace2-pytorch`, 2018.

48. DeVries, T. and Taylor, G.: Improved regularization of convolutional neural networks with cutout. 08 2017.

CITED LITERATURE (continued)

49. Milletari, F., Navab, N., and Ahmadi, S.-A.: V-net: Fully convolutional neural networks for volumetric medical image segmentation. pages 565–571, 10 2016.

VITA

NAME	Guglielmo Menchetti
EDUCATION	
	Master of Science in “Computer Science”, University of Illinois at Chicago, May 2020, USA
	Master of Science in “Computer Science and Engineering”, Politecnico di Milano, December 2020, Italy
	Bachelor’s Degree in ”Computer Science and Engineering””, Università degli Studi di Firenze, April 2017, Italy
LANGUAGE SKILLS	
Italian	Native speaker
English	Full working proficiency
	2017 - IELTS examination (7/9)
	A.Y. 2018/20 - One Year of study abroad in Chicago, Illinois
	A.Y. 2017/18 - Lessons and exams attended exclusively in English
SCHOLARSHIPS	
Spring-Fall 2019	Research Assistantship (RA) position (10 hours/week) with full tuition waiver plus monthly stipend
Spring 2018	Italian scholarship for TOP-UIC students